JOURNAL OF MAGNETIC RESONANCE 21, 387–396 (1976)

The Divacancy in Silicon: Spin–Lattice Relaxation and Passage Effects in Electron Paramagnetic Resonance

C. A. J. AMMERLAAN AND A. VAN DER WIEL

Natuurkundig Laboratorium der Universiteit van Amsterdam, Valckenierstraat 65, Amsterdam-C, The Netherlands

Received April 7, 1975

The longitudinal spin–lattice relaxation time T_1 of the divacancy in silicon, in its positively charged state, was determined in the temperature region between 10 and 30 K. The study was made by measuring the line shape and amplitude of the electron paramagnetic resonance spectrum of V_2^+ (the Si–G6 spectrum) in a static magnetic field of 8.24 kOe. The passage conditions in observing the resonances were varied through the transition from adiabatic fast ($\omega_m T_1 > 1$) to adiabatic slow ($\omega_m T_1 < 1$) with respect to the audiofrequency (ω_m) modulation field. Explicit formulas are derived to describe line shape and amplitude of the resonance in the transition region around $\omega_m T_1 = 1$. The spin–lattice relaxation time found is given by $T_1(\mathrm{s}) = 3.4 \times 10^5 \times T(\mathrm{K})^{-6.6}$, which demonstrates that the Raman two-phonon process is the active relaxation mechanism.

INTRODUCTION

The divacancy is one of the prominent radiation damage centers in silicon. Contrary to the simpler intrinsic defects, the lattice vacancy and the interstitial, the divacancy has zero mobility at room temperature. Divacancies are easily produced, rather uniformly distributed as stable and isolated defects, by a room temperature electron irradiation. Thanks to these favorable circumstances divacancies in silicon are already intensively investigated. Mainly spectroscopic techniques were used in the experimental studies: infrared absorption (*1–4*), photoconductivity (*5–9*), electron paramagnetic resonance (EPR) (*10–13*), and electron-nuclear double resonance (ENDOR) (*14*). From motional effects (*2, 3, 12*) and annealing behavior (*2, 4, 12, 15, 16*) the migrational properties and stability of this defect were derived. Though therefore the divacancy is a well-investigated defect spin–lattice relaxation rates of it have never been reported.

Depending upon the Fermi level the divacancy will assume one of four possible charge states, ranging from singly positive in *p*-type to doubly negative in *n*-type silicon. Three energy levels located in the bandgap are associated with the divacancy (*12*). Divacancies may be embedded in the host silicon crystal in twelve distinct orientations. For each of the four possible vacancy–vacancy axes in the silicon lattice (⟨111⟩-directions) there exist three atomic configurations slightly differing by a Jahn–Teller distortion.

In its positively charged state the divacancy, V_2^+, is a paramagnetic center. Arising from a single unpaired electron spin the center has $S = \frac{1}{2}$. The corresponding EPR spectrum was designated Si–G6 (*17*). The angular dependence of the resonance lines is conveniently described by the spin-Hamiltonian $\mathcal{H} = \beta \mathbf{H} \cdot \mathbf{g} \cdot \mathbf{S}$, with principal

g-tensor components $g_1 = 2.0004$, $g_2 = 2.0020$, and $g_3 = 2.0041$. Hyperfine interactions with ^{29}Si nuclei, located close to the divacancy in the silicon crystal, are the origin of inhomogeneous broadening of the resonance. In a regular EPR experiment the greater part of this broadening is not resolved leading to a full linewidth at half maximum (FWHM) between 1.5 and 2.0 Oe.

A resonance spectrum of V_2^+, as recorded for $\mathbf{H}\|\langle 100\rangle$, is shown in Fig. 3a. In this particular direction of the magnetic field $\mathbf{H}$, along a high symmetry crystallographic axis, resonance lines corresponding to four of the divacancy orientations coincide at the low field resonance ($\simeq 8230$ Oe). The divacancies in the remaining eight orientations also yield only one resonance line at the higher field ($\simeq 8240$ Oe).

Resonance conditions are specified by two internal parameters, which are determined by the nature of the paramagnetic center and the environment to which it is coupled. These are the inhomogeneous linewidth ΔH and the spin–lattice relaxation time T_1. Knowledge of these two parameters is required to perform a magnetic resonance experiment (EPR or ENDOR) under well-controlled conditions.

In this paper we report a study of the spin–lattice relaxation of the divacancy in the positively charged state. The longitudinal spin–lattice relaxation time T_1 was measured in the temperature interval between 10 and 30 K. The experimental method consisted of observing the line shapes and amplitudes of the EPR signal under various passage conditions. To analyze the results formulas were derived which are continuously valid in the region around $\omega_m T_1 = 1$. In this region the passage conditions change from adiabatic slow ($\omega_m T_1 < 1$) to adiabatic fast ($\omega_m T_1 > 1$) with respect to the audio-frequency modulation of the magnetic field. This is elaborated in the next section of this paper. Application of the theoretical development to the determination of the spin–lattice relaxation time of V_2^+ is described subsequently.

LINE SHAPES

In a magnetic resonance experiment spectra are usually recorded keeping the microwave frequency at a constant value ω_0, while the magnetic field is slowly swept to satisfy the resonance condition $\hbar\omega_0 = g\beta H_0$. The magnetic field H is composed of a static field H_0 and a component $H't$ which varies linearly in time with scan rate H': $H = H_0 + H't$. Time and magnetic field scale are fixed by the requirement that $t = 0$, $H = H_0$ are at the center of the resonance. From the resonance condition one finds $\omega_0 = \gamma H_0$, with γ representing the gyromagnetic ratio. For $g = 2$, as is nearly the case for unpaired divacancy electrons in silicon, $\gamma = g\beta/\hbar = 1.76 \times 10^7$ Oe^{-1} s^{-1}. On the slowly varying external field H the modulation field $H_m \sin\omega_m t$ is superposed. The microwave field, with amplitude $2H_1$ and frequency ω_0, is applied at right angles to the external field.

Inhomogeneous broadening of the resonance lines arises from hyperfine interactions with ^{29}Si nuclei, present in any normal crystal with the natural abundance of 4.7%. To be specific we assume a Gaussian distribution of the hyperfine fields H_{hf}, expressed by

$$w(H_{hf}) = (1/\Delta H(2\pi)^{1/2}) \exp(-H_{hf}^2/2\Delta H^2),$$

with the total probability normalized to unity. For the high field $\mathbf{H}\|\langle 100\rangle$ resonance of the positive divacancy in silicon the linewidth ΔH equals 0.85 Oe.

Resonance conditions are characterized by seven parameters. Two of these are the internal parameters already mentioned in the introduction: the hyperfine width ΔH and the spin–lattice relaxation time T_1. Apart from these there are five external parameters: static magnetic field H_0, scan rate H', microwave field H_1, modulation field amplitude H_m, and modulation frequency ω_m. Without loss of generality the number of line shape parameters may be reduced from seven to five by defining the new dimensionless quantities $h_0 = H_0/\Delta H$, $h_1 = H_1/\Delta H$, $h_m = H_m/\Delta H$, $\omega_m T_1$ and $\mu = T_1 H'/H_1$. We also introduce $h = H' t/\Delta H = (H - H_0)/\Delta H$.

Our derivation of line shapes is based on the Bloch equations (*18*). In our samples the concentration of divacancies is low. Dipolar interaction fields between the paramagnetic centers are therefore small compared to the microwave field. In this case it is allowed to ignore spin–spin relaxation and to put the transverse relaxation time T_2 equal to the longitudinal relaxation time T_1 (*19*). The solution of the Bloch equations is facilitated by introducing the rotating coordinate system. The linearly polarized microwave field is decomposed into two oppositely rotating components. Only one of these needs to be considered as long as $h_1 \ll h_0$ and $|h| \ll h_0$, assumptions which are readily met in practice. A solution of Bloch's differential equations in terms of certain integrals was obtained by Portis (*20*). The results are only valid if the passage through resonance is adiabatic, i.e. for $H' \ll \gamma H_1^2$ and $\omega_m H_m \ll \gamma H_1^2$, and saturation of the resonance: $\gamma H_1 T_1 \gg 1$. Again these conditions are easily met. In adiabatic passage through resonance the magnetization will remain parallel to the effective field in the rotating frame. From this fact it follows that the absorption component χ'' of the magnetic susceptibility χ will be negligible in comparison with the dispersion component χ'. Two further assumptions need to be made in order to proceed and to arrive at useful expressions. The first of these, $h_m \ll h_1$, allows a series expansion of integrands to be made as a power series of h_m/h_1. In the results to be presented only the leading term in this expansion is retained. The second approximation, $\mu \ll \omega_m T_1$, implies a slow linear scan compared to the modulation. This assumption enables one to evaluate certain integrals by repeated integration by parts.

A result reached finally for χ'_{90}, which is the component of the dispersion 90° out of phase with the applied modulation, reads:

$$\chi'_{90}(h) = \frac{-1}{2(2\pi)^{1/2}} \cdot \chi_0 h_0 \frac{h_m}{h_1} \frac{\omega_m T_1}{1 + \omega_m^2 T_1^2} \int_{-\infty}^{+\infty} dx \cdot \frac{1}{(1+x^2)^2} \exp\{-(h_1 x - h)^2/2\}.$$

The symbol χ_0 here represents the static paramagnetic susceptibility. The remaining integral is conveniently handled by series expansion, yielding

$$\chi'_{90}(h) = -\tfrac{1}{8}(2\pi)^{1/2} \chi_0 h_0 \frac{h_m}{h_1} \frac{\omega_m T_1}{1 + \omega_m^2 T_1^2} \exp(-h^2/2) \cdot \{C_2 + \tfrac{1}{2}(2C_1 - C_2) h_1^2 h^2 + \mathcal{O}(h^4)\}, \quad [1]$$

where the functions C_n, defined by

$$C_n(h_1) = \frac{2^{2n-2}\{(n-1)!\}^2}{\pi(2n-2)!} \int_{-\infty}^{+\infty} dx \cdot \frac{1}{(1+x^2)^n} \exp(-h_1^2 x^2/2),$$

are related to the complementary error function:

$$C_1(h_1) = \operatorname{erfc}(h_1/\sqrt{2}) \cdot \exp(h_1^2/2),$$
$$C_2(h_1) = h_1(2/\pi)^{1/2} + (1 - h_1^2)\, C_1, \text{ etc.}$$

A symmetrical line shape is predicted by these formulas. For the special case $h_1 \ll 1$ the equations take the much simpler form:

$$\chi'_{90}(h) = -\tfrac{1}{8}(2\pi)^{1/2}\, \chi_0\, h_0 \frac{h_m}{h_1} \frac{\omega_m T_1}{1 + \omega_m^2 T_1^2} \exp(-h^2/2). \qquad [2]$$

The resonance line shape is a reproduction of the hyperfine envelope. The validity of the expressions is restricted to the interior of the volume shown hatched in Fig. 1. Also

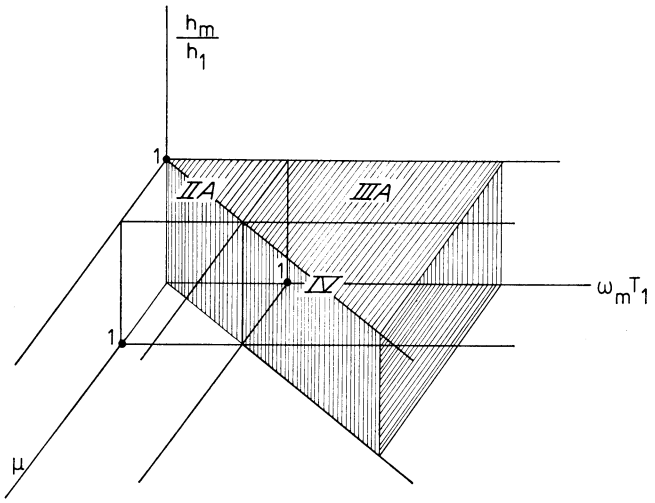

FIG. 1. The expressions for χ'_{90} are valid inside the hatched volume. Roman numerals indicate the passage cases distinguished by Portis (*20*).

indicated in this figure are the ranges of validity of various passage cases as considered by Portis (*20*). An important thing to note is the applicability of our expressions continuously across the boundary $\omega_m T_1 = 1$. For $\omega_m T_1 \gg 1$ the passage through resonance is called fast as the spin packets do not relax considerably between successive modulation cycles. For slow passage, i.e., not fast passage, the modulation period is long compared to the relaxation time T_1 (*21*, *22*). The restraint $h_m \ll h_1$ is an annoying one as it limits the experiments to conditions where the signal is small. On the other hand the restriction $\mu \ll \omega_m T_1$ is automatically satisfied in the usual experimental circumstances.

For χ'_0, which is the dispersion component of the magnetic susceptibility in phase with the magnetic field modulation, results are more complicated. However, for conditions of slow linear scan, i.e. for $\mu \ll 1$, we obtain:

$$\chi'_0(h) = \tfrac{1}{8}(2\pi)^{1/2}\, \chi_0\, h_0 \frac{h_m}{h_1} \exp(-h^2/2) \cdot \left\{ \frac{C_2}{1 + \omega_m^2 T_1^2} - 2C_1 + C_2 + \tfrac{1}{2}\left(\frac{2C_1 - C_2}{1 + \omega_m^2 T_1^2} + 4C_1 - C_2 - \frac{2}{h_1}\left(\frac{2}{\pi}\right)^{1/2} \right) h_1^2 h^2 + \mathcal{O}(h^4) \right\}. \qquad [3]$$

Depending on the values of $\omega_m T_1$ and h_1 this formula describes a variety of resonance line shapes. Examples are shown in Fig. 2. All line shapes are symmetric with respect to $H = H_0$, a result that no longer holds true for $\mu \gtrsim 1$. Curve a represents the boundary between the regions with positive or negative resonance signal at $t = 0$, $H = H_0$. This curve is given by the equation:

$$\omega_m T_1 = \{2(C_2 - C_1)/(2C_1 - C_2)\}^{1/2}. \quad [4]$$

Curve b in Fig. 2 separates the regions with and without a positively directed dip around $t = 0$ in the otherwise negative signal.

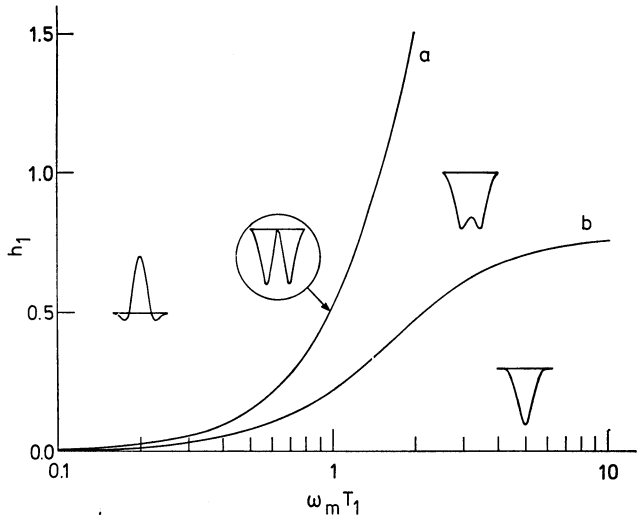

FIG. 2. Typical line shapes of χ_0' for the passage conditions $H_m \ll H_1$, $\mu \ll \omega_m T_1$, and $\mu \ll 1$.

EXPERIMENTAL METHOD

For our experiments *p*-type silicon, doped with 5×10^{16} boron atoms per cm^3 and with a dislocation density of 2×10^4 cm^{-2}, was used as starting material (*23*). Samples were irradiated with 1.5 MeV electrons at room temperature. A total dose of 1.0×10^{18} electrons per cm^2 was divided equally on two opposite sides to enhance the uniformity of defect production. This resulted in a density of divacancies of 8×10^{15} cm^{-3} (*24*). Defect production was monitored by measuring the resistivity, which rose from a pre-irradiation room temperature value of 0.34 Ohm·cm to a final 3.3 Ohm·cm. The samples remained *p*-type, as confirmed by hot point checks, ensuring that divacancies were in the positive charge state.

Magnetic resonance experiments were carried out in a superheterodyne spectrometer operating in the *K*-band. For our microwave frequency of 23.1 GHz and for $g = 2$ resonances are found at $H = 8250$ Oe. The spectrometer was tuned to observe the dispersion signal. Phase sensitive detection with the audiofrequency modulation component of the magnetic field was employed.

The microwave cavity was a cylinder with height equal to the diameter, resonating in the TE011 mode. The silicon sample was also cylindrical in shape; it was ground

to a diameter of 1.5 mm and cut to a height of 3.0 mm. This small sample was mounted along the cavity axis and in the middle of the cavity, supported by a pedestal consisting of a thin fused quartz rod. In this way the whole of the sample volume is in the region of nearly uniform and maximum microwave field. The cavity was coupled critically to the waveguide. This allows the microwave field $2H_1$ inside the cavity to be calculated from the power incident upon the cavity and from its quality factor Q. The Q of the cavity, which depended weakly on temperature, was determined from the cavity bandwidth. In actual experiments H_1 equalled 0.5 Oe.

To avoid screening of the modulation field by the skin effect a thin walled silver coated epibond cavity was constructed. The modulation field amplitude H_m was calibrated, for all modulation frequencies used, by a pickup coil located in the center of the cavity. Experiments were performed with $H_m = 0.1$ Oe.

The temperature of the sample was measured with a Au(0.03% Fe)–Chromel thermocouple fastened to the cavity bottom. Temperatures could be raised with the help of a resistance heater wound bifilar around the copper cavity bottom. While recording resonances the temperature was kept constant within 0.1 K.

A reference sample, a tiny piece of heavily phosphorus doped silicon showing the isotropic conduction electron line at $g = 1.99875$ (*25*), was also mounted in the cavity. This sample served the purpose of phase reference and of check on the variation of sensitivity with temperature due to the Boltzmann factor.

In all measurements the static magnetic field $\mathbf{H}_0$ was parallel to a $\langle 100 \rangle$ crystallographic axis of the sample containing the divacancies.

RESULTS

To apply the formulas of the section on line shapes the actual experimental passage conditions must be in agreement with the underlying assumptions. Values of the external parameters as realized in the experiments were $H_1 = 0.5$ Oe, $H_m = 0.1$ Oe, and $H' = 0.17$ Oe/s. All resonances were recorded under conditions of adiabatic passage and of saturation. The condition $\mu \ll \omega_m T_1$, which is equivalent to $H' \ll \omega_m H_1$ and therefore independent of T_1 and the temperature, is also satisfied.

Most information on spin–lattice relaxation was obtained by observing the 90° out of phase signal. A typical χ'_{90} resonance spectrum is shown in Fig. 3a. The line shape resembles the Gaussian hyperfine envelope, as predicted by Eqs. [1] and [2]. A slight broadening occurs because H_1 is not small compared to the hyperfine linewidth ΔH. From the full width at half maximum we deduce $\Delta H = 0.85$ Oe. The maximum amplitude at $h = 0$ is given by (Eq. [1]):

$$|\chi'_{90}(0)| = \tfrac{1}{8}(2\pi)^{1/2} \chi_0 h_0 \frac{h_m}{h_1} \frac{\omega_m T_1}{1 + \omega_m^2 T_1^2} C_2.$$

The variation of amplitude with temperature is governed by the factor $\omega_m T_1/(1 + \omega_m^2 T_1^2)$, and is independent of μ, h_1, and h_m. Therefore an exact knowledge of these parameters is not required, an approximate knowledge, to judge whether the passage conditions are satisfied, suffices. The χ'_{90} signal amplitude reaches a maximum for the temperature for which $\omega_m T_1 = 1$; then $\omega_m T_1/(1 + \omega_m^2 T_1^2)$ equals 0.5. For both larger and smaller T_1, corresponding to lower and higher temperatures respectively, the signal amplitude is smaller. In Fig. 4 the temperature dependence of $\chi'_{90}(0)$ is shown for four different

values of the modulation frequency $f_m = \omega_m/2\pi$. The modulation frequencies applied in the experiments were $f_m = 19.6$, 81.9, 323, and 1521 Hz. The maxima of the curves are normalized to the theoretical 0.5. From each curve, using the relationship $\chi'_{90}(0)$

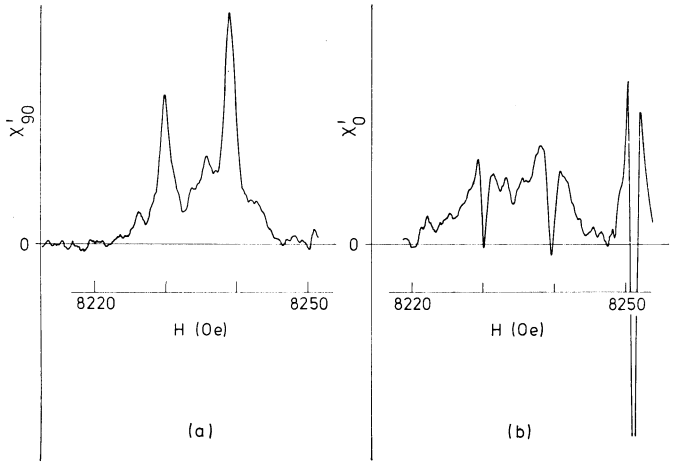

FIG. 3. Experimental divacancy spectra: (a) the 90° out of phase signal χ'_{90}, (b) the in phase signal χ'_0 under passage conditions for which $\chi'_0(0) \simeq 0$.

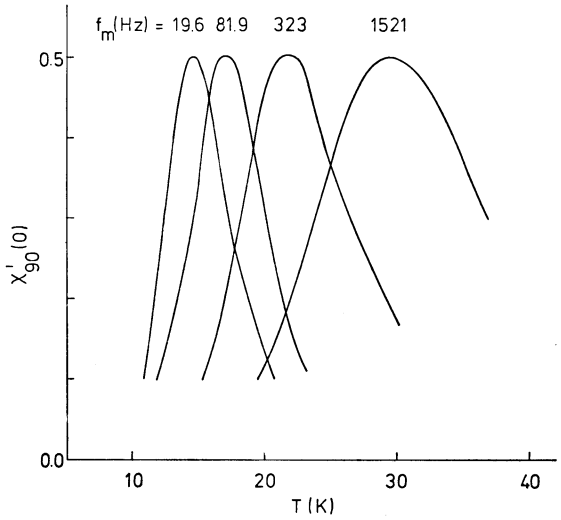

FIG. 4. The temperature dependence of $\chi'_{90}(0)$ for various modulation frequencies f_m.

is proportional to $\omega_m T_1/(1 + \omega_m^2 T_1^2)$, the relaxation time T_1 may then be calculated as function of the temperature over the range of the measurements. Results of these calculations yield the four straight lines, which, labeled with the relevant modulation frequency, are presented in Fig. 5.

Some additional information was obtained by observing the in phase component χ'_0 under conditions of slow linear scan: $\mu \ll 1$. At low temperatures the signal is negative,

or in equivalent terms 180° out of phase (*20*). Upon increasing the temperature a positive dip around $h = 0$ appears in the signal. This starts from the passage conditions represented by curve b in Fig. 2. For still higher temperatures the conditions of curve a in Fig. 2 are reached. Under these passage conditions $\chi_0'(0) = 0$, which gives the easily recognizable line shape as shown encircled in Fig. 2. An experimentally observed spectrum for this particular case is reproduced in Fig. 3b, together with a trace of the reference signal as a phase marker. For the highest temperatures the signal is positive,

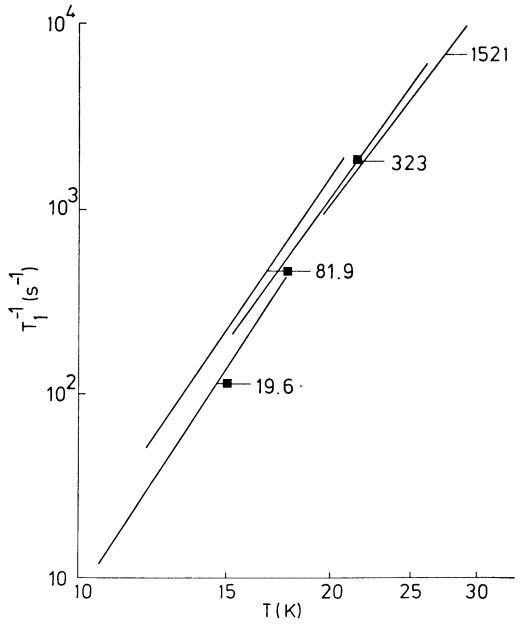

FIG. 5. The reciprocal of the spin–lattice relaxation time T_1 of the positive divacancy in silicon as function of the temperature T. Modulation frequencies are labels to the curves, black squares (■) represent the χ_0' results.

or 0° out of phase, for most of the time, and has a shape which is typical for a dispersion derivative. In our experiments conditions of slow linear scan, $\mu \ll 1$, were realized. The transition from negative to positive $\chi_0'(0)$, curve a in Fig. 2, is then given by Eq. [4]. To utilize this relation for a determination of T_1 it is necessary to know h_1 as C_1 and C_2 are functions of this parameter. In our experimental case $H_1 = 0.5$ Oe and $\Delta H = 0.85$ Oe, from which it follows that $\omega_m T_1 = 1.1$ for $\chi_0'(0) = 0$. This fact allows one to determine T_1 for one temperature for every modulation frequency. Results of this measurement procedure are shown separately in Fig. 5, and are seen to support the χ_{90}' results.

A least-squares adjustment of all experimental data to a formula of the type $T_1^{-1} = aT^b$ was made. The result, valid in the temperature interval 10 K $< T <$ 30 K, is $a = 2.9 \times 10^{-6}$ s^{-1}, $b = 6.6$, with the temperature T expressed in Kelvin. For this analysis only data from the higher field resonance for $\mathbf{H}_0 \| \langle 100 \rangle$ were used. The smaller line at lower magnetic field, corresponding to four divacancy orientations, yielded results identical within experimental error.

DISCUSSION

From the temperature dependence of the relaxation time we conclude that the Raman two-phonon process is the active spin–lattice relaxation mechanism. In Raman scattering one phonon is absorbed, while subsequently a phonon with energy differing by the Zeeman splitting is emitted. The whole process results in spin flip with conservation of total energy (*26*). Dependent on conditions the Raman process will reveal itself by a typical variation with temperature (*26–30*). A theoretically predicted seventh power law is frequently observed. Our power law exponent, $b = 6.6$, is slightly lower than this theoretical value. This discrepancy is partly due to the fact that temperatures in our experiments were not always low compared to the Debye temperature of transverse phonons in silicon, $\theta_t = 212$ K (*31*).

Not much is known about spin–lattice relaxation of other radiation induced defects in silicon. For the substitutional oxygen impurity (*A*-center) much longer relaxation times were observed for T between 2 and 4 K (*32*).

Contrary to this unsatisfying situation spin–lattice relaxation processes of shallow donor electrons are rather well understood. For these impurities direct, Raman, and Orbach relaxation mechanisms were identified experimentally by the corresponding characteristic temperature dependences (*30*, *33–35*). Also the effect of the magnetic field strength and the anisotropy of the spin–lattice relaxation, i.e. its dependence upon the orientation of the magnetic field with respect to the crystal axes, were studied (*36*). The theoretical description of spin–lattice relaxation here is quite satisfactory (*30*, *37–39*). Preliminary experimental data indicate that a similar wealth of phenomena is to be expected for the deep level defects. Its further exploration and explanation is left to future research.

REFERENCES

1. H. Y. Fan and A. K. Ramdas, *J. Appl. Phys.* **30,** 1127 (1959).
2. L. J. Cheng, J. C. Corelli, J. W. Corbett, and G. D. Watkins, *Phys. Rev.* **152,** 761 (1966).
3. L. J. Cheng and P. Vajda, *Phys. Rev.* **186,** 816 (1969).
4. C. S. Chen and J. C. Corelli, *Phys. Rev.* **B5,** 1505 (1972).
5. L. J. Cheng, *Phys. Letters* **24A,** 729 (1967).
6. A. H. Kalma and J. C. Corelli, *Phys. Rev.* **173,** 734 (1968).
7. L. J. Cheng, "Radiation Effects in Semiconductors," Plenum, New York, 1968, p. 143.
8. P. Vajda and L. J. Cheng, *Radiation Effects* **8,** 245 (1971).
9. R. C. Young and J. C. Corelli, *Phys. Rev.* **B5,** 1455 (1972).
10. J. W. Corbett and G. D. Watkins, *Phys. Rev. Letters* **7,** 314 (1961).
11. G. Bemski, B. Szymanski, and K. Wright, *J. Phys. Chem. Solids* **24,** 1 (1963).
12. G. D. Watkins and J. W. Corbett, *Phys. Rev.* **138,** A543 (1965).
13. C. A. J. Ammerlaan and G. D. Watkins, *Phys. Rev.* **B5,** 3988 (1972).
14. J. G. de Wit, C. A. J. Ammerlaan, and E. G. Sieverts, "Lattice Defects in Semiconductors, 1974," The Institute of Physics, London, p. 178.
15. L. J. Cheng and J. Lori, *Phys. Rev.* **171,** 856 (1968).
16. D. F. Daly and H. E. Noffke, *Radiation Effects* **10,** 191 (1971).
17. G. D. Watkins, "Radiation Damage in Semiconductors," Dunod, Paris, 1965, p. 97.
18. F. Bloch, *Phys. Rev.* **70,** 460 (1946).
19. A. G. Redfield, *Phys. Rev.* **98,** 1787 (1955).
20. A. M. Portis, Technical Note No. 1, Sarah Mellon Scaife Radiation Laboratory, University of Pittsburgh, Pittsburgh, Pennsylvania, U.S.A., 1955.
21. M. Weger, *Bell System Tech. J.* **39,** 1013 (1960).
22. R. S. Alger, "Electron Paramagnetic Resonance," Interscience Publishers, New York, 1968.

23. Silicon was supplied by Wacker-Chemitronic.
24. J. W. CORBETT AND G. D. WATKINS, *Phys. Rev.* **138,** A555 (1965).
25. G. FEHER, *Phys. Rev.* **114,** 1219 (1959).
26. K. J. STANDLEY AND R. A. VAUGHAN, "Electron Spin Relaxation Phenomena in Solids," Adam Hilger Ltd., London, 1969.
27. J. C. VERSTELLE AND D. A. CURTIS, "Paramagnetic Relaxation", *in* "Encyclopedia of Physics," Springer–Verlag, Berlin, 1968, p. 1.
28. E. ABRAHAMS, *Phys. Rev.* **107,** 491 (1957).
29. R. ORBACH AND M. BLUME, *Phys. Rev. Letters* **8,** 478 (1962).
30. T. G. CASTNER, JR., *Phys. Rev.* **130,** 58 (1963).
31. R. A. SMITH, "Semiconductors," University Press, Cambridge, 1959.
32. O. G. KOSHELEV, YU. P. KOVAL, AND YA. G. KLYAVA, *Soviet Phys. Semiconductors* **1,** 1057 (1968).
33. G. FEHER AND E. A. GERE, *Phys. Rev.* **114,** 1245 (1959).
34. A. HONIG AND E. STUPP, *Phys. Rev.* **117,** 69 (1960).
35. T. G. CASTNER, JR., *Phys. Rev. Letters* **8,** 13 (1962).
36. D. K. WILSON AND G. FEHER, *Phys. Rev.* **124,** 1068 (1961).
37. H. HASEGAWA, *Phys. Rev.* **118,** 1523 (1960).
38. L. ROTH, *Phys. Rev.* **118,** 1534 (1960).
39. T. G. CASTNER, *Phys. Rev.* **155,** 816 (1967).